DOI: 10.1021/ma901685p

Macromolecules
ARTICLE

# Polyisobutylene RAFT CTA by a Click Chemistry Site Transformation Approach: Synthesis of Poly(isobutylene-*b*-*N*-isopropylacrylamide)

**Andrew J. D. Magenau, Nemesio Martinez-Castro, Daniel A. Savin, and Robson F. Storey***

*School of Polymers and High Performance Materials, The University of Southern Mississippi, Box 10076, Hattiesburg, Mississippi 39402*

*Received July 29, 2009; Revised Manuscript Received September 2, 2009*

ABSTRACT: A novel block copolymer, composed of polyisobutylene (PIB) and poly(*N*-isopropylacrylamide) (PNIPAM) segments, was synthesized. The PIB block was prepared via quasiliving cationic polymerization and end-functionalized by in-situ quenching to yield telechelic halogen-terminated PIB. Azido functionality was obtained by displacement of the terminal halogen through nucleophilic substitution, which was confirmed by both $^{1}$H and $^{13}$C NMR. Coupling of an alkyne-functional chain transfer agent (CTA) to azido PIB was successfully accomplished through a copper-catalyzed click reaction. Structure of the resulting PIB-based macro-CTA was verified with $^{1}$H NMR, FTIR, and GPC, whereas coupling reaction kinetics were monitored by real-time variable temperature (VT) $^{1}$H NMR. Subsequently, the function of this macro-CTA was demonstrated by RAFT polymerization of NIPAM for synthesis of the second block. RAFT kinetics was investigated under a variety of reaction conditions using VT NMR, and the resulting block copolymers were characterized by $^{1}$H NMR and GPC. Aqueous solution properties were probed by dynamic light scattering confirming the presence of self-assembled aggregates with reversible temperature-sensitive responsiveness.

## Introduction

Development of controlled/living polymerizations has enabled synthetic polymer chemists to design complex polymeric architectures with great precision.[1] Block copolymers in particular have gained significant attention because of their unique material properties resulting from compositionally different block segments and the ability to self-assemble into highly organized structures.[2] Self-assembling materials have many potential applications, both as dispersions and in the solid state, due to their ability to form versatile and functional morphologies.[1] Thus, block copolymer systems are being developed for and have found numerous applications in the areas of biomedical devices,[3−6] biomaterials,[4,7,8] thermoplastic elastomers (TPEs),[9] fuel cells,[10,11] and electronics.[12,13]

Polyisobutylene (PIB) is a completely saturated hydrocarbon rubber that can only be produced through cationic polymerization. Inherent attractive properties of this synthetic elastomer are its exceptional oxidative and chemical resistance, superior gas barrier and mechanical damping characteristics, and excellent biocompatibility. Because of these properties PIB-based block copolymers have continued to be a topic of great interest. Poly(styrene-*b*-isobutylene-*b*-styrene) (SIBS) block copolymer has found a niche market as a biomaterial and is used as the matrix polymer for the drug-containing coating on a commercial drug-eluting coronary stent.[7,14−16] Recently, prospective materials for biotechnology and medicine were created from self-assembling PIB-based polymersomes and micelles, creating novel delivery/encapsulation systems[17,18] and interpolyelectrolyte complexes.[19] In addition, Kennedy et al. have recently developed PIB-based segmented thermoplastic polyurethane/ureas (TPUs) exhibiting unprecedented resistance to oxidative/hydrolytic degradation for long-term medical applications.[20,21] In other areas, novel PIB-based TPEs with poly(ether ketone) outer blocks for increased thermal stability,[22] and dendritic PIB-core TPEs with carbon black and silica fillers for increased mechanical properties, were synthesized.[23]

PIB-based block copolymers have been synthesized by four different strategies: sequential monomer addition, macromolecular coupling, dual-site initiators,[24] and site transformation.[9] Sequential monomer addition offers unparalleled simplicity but, in the case of PIB-based block copolymers, allows combinations of cationically polymerizable monomers only. This selection of monomers is confined essentially to isobutylene, isoprene, vinyl ethers, styrenics, and *N*-vinylcarbazole, and the process is no longer simple when the monomer pair exhibit large reactivity differences.[25] Macromolecular coupling[17,26] of previously fabricated functional polymers requires quantitative functionalization of the chain ends of both polymers, a high-conversion coupling reaction, and a common solvent system; otherwise, the yield of the desired block copolymer is low, and a tedious separation of homopolymers is often involved. Dual-site initiators contain initiating sites for two mechanistically different polymerizations and require no intermediate transformation steps to affect the second polymerization after the first. Site transformation involves conversion of the head or tail group of the PIB block segment into an initiator for a mechanistically different chain polymerization process. This technique effectively expands the library of polymers segments that can be mated to PIB. Block copolymer synthesis using site transformation has been successfully demonstrated with atom transfer radical polymerization (ATRP),[27−29] condensation polymerization,[30] anionic polymerization,[31,32] and most recently by reversible addition−fragmentation chain transfer (RAFT) polymerization.[33]

RAFT has proven to be very versatile regarding monomers, solvents, and reaction conditions and yields macromolecules with predetermined molecular weights and narrow polydispersities.[34,35] Because of its versatility and capability to polymerize many monomers that are inherently troublesome for other polymerization techniques, RAFT is potentially an ideal polymerization

*Corresponding author: E-mail Robson.Storey@usm.edu; Tel 601-266-4879; Fax 601-266-5635.

 Published on Web 09/17/2009 

technique to combine with cationic polymerization by site transformation. In addition, chain transfer agents (CTAs) used in the RAFT process can be synthesized to carry many useful reactive end groups including azide[36] and alkyne[37] for copper(I)-catalyzed Huisgen [3 + 2] dipolar cycloadditions. This reaction, catagorized by Sharpless et al. as a "click" reaction, is known to be quantitative, devoid of side reactions and byproducts, tolerant to a wide range of functional groups, and requiring only mild reaction conditions.[38,39] Because of these attributes, the azide/alkyne reaction has received significant attention in macromolecular chemistry and has found use in specific systems for postpolymerization functionalization, novel polymer synthesis, and chain extension for block copolymer synthesis.[40]

Stimuli-responsive block copolymers are of immense importance and have attracted significant attention as "smart" materials.[41] Poly(*N*-isopropylacrylamide) (PNIPAM) is known to display a sharp, thermally reversible phase transition in aqueous solution at ~32 °C.[42] Investigation of this phase transition has revealed that PNIPAM macromolecules experience dehydration and collapse from a hydrated, extended coil to a hydrophobic globule, upon raising the temperature through the cloud point, ultimately resulting in intermolecular aggregation.[43] Various hydrophobically modified PNIPAM-based polymers have been reported in the literature and are being studied for many potential applications.[44] Functional PNIPAMs have been synthesized to be joined with various hydrophobic polymer blocks including, for example, polystyrene[45,46] and tetrahydrofuran-protected 2-hydroxyethyl methacrylate[47] as well as alkyl groups,[48] alkyl chain transfer agents,[49] and chromophores.[50] Herein, we report the synthesis of a novel amphiphilic diblock copolymer, composed of PIB and PNIPAM segments, through the combination of quasiliving cationic polymerization and RAFT by a click chemistry site transformation approach.

## Experimental Section

**Materials.** Hexane (anhydrous, 95%), 2,6-lutidine (redistilled, 99.5%), $TiCl_4$ (99.9%, packaged under $N_2$ in sure-seal bottles), chloroform-*d* (99.8 atom % D), DMF (anhydrous, 99.8%), bromotris(triphenylphosphine)copper(I) ($(Ph_3P)_3CuBr$) (98%), and 1,3,5-trioxane (≥99%) were purchased from Sigma-Aldrich and used as received. 1-(3-Bromopropyl)pyrrole (PyPBr) (>95%, TCI America), THF, heptanes, and dioxane (all Sigma Aldrich) were distilled from calcium hydride under a $N_2$ atmosphere. *N*-Isopropylacrylamide (NIPAM; 97%, Sigma-Aldrich) was recrystallized twice from a hexane/benzene mixture (3/2, v/v). 2,2′-Azobis(2-methylpropionitrile) (AIBN; 98%, Sigma-Aldrich) (AIBN) was recrystallized twice from ethanol. Isobutylene (IB) (BOC, 99.5%) and $CH_3Cl$ (99.95%, Alexander Chemical Corp.) were dried by passing the gaseous reagent through columns packed with $CaSO_4$ and $CaSO_4$/4 Å molecular sieves, respectively, and condensed within a $N_2$-atmosphere glovebox immediately prior to use. 2-Chloro-2,4,4-trimethylpentane (TMPCl) was prepared by bubbling HCl gas through neat 2,4,4-trimethyl-1-pentene (99%, Sigma-Aldrich) at 0 °C. The HCl-saturated TMPCl was stored at 0 °C and immediately prior to use was neutralized with $NaHCO_3$, dried over anhydrous $MgSO_4$, and filtered. Alkyne-functional CTA, propargyl 2-(1-dodecylsulfanylthiocarbonylsulfanyl)-2-methylpropionate, was synthesized as previously reported.[37]

**Synthesis of 1-(3-Azidopropyl)pyrrole-Terminated PIB (PIB-$N_3$).** Three 1-(3-bromopropyl)pyrrole-terminated PIB precursors (Table 1) were synthesized by quenching TMPCl-initiated quasiliving IB polymerizations with 1-(3-bromopropyl)pyrrole.[51] A representative procedure to produce $PIB_{44}$-Br was as follows. Quasiliving polymerization of IB with TMPCl as an initiator was carried out within a $N_2$ atmosphere glovebox, equipped with an integral, cryostated hexane/heptanes bath. Into a round-bottom flask equipped with a mechanical stirrer, infrared probe, and thermocouple were added 144 mL of $CH_3Cl$, 216 mL of hexane, and 0.15 mL (0.14 g, 1.3 mmol) of 2,6-lutidine. The mixture was allowed to equilibrate to −70 °C, and then 20.4 mL (14.2 g, 0.254 mol) of IB was charged to the reactor. After thermal equilibration, 1.113 mL (0.9730 g, 6.545 mmol) of TMPCl was added to the reactor. To begin the polymerization, 2.16 mL (3.74 g, 0.0197 mol) of $TiCl_4$ was charged to the reactor. Full monomer conversion (>98%) was achieved in 40 min, after which time a prechilled solution of PyPBr, prepared by dissolving 1.81 mL of PyPBr (2.46 g, 13.1 mmol) into 25 mL of hexane/$CH_3Cl$ (60/40, v/v, −70 °C), was added to the polymerization. PyPBr was allowed to react with the living chain ends for 40 min. Finally, the reaction was quenched by addition of excess prechilled methanol. The contents of the reaction flask were allowed to warm to room temperature, and the polymer in hexane was immediately washed with methanol and then precipitated into methanol from hexane. The precipitate was collected by dissolution in hexane; the solution was washed with water, dried over $MgSO_4$, and concentrated on a rotary evaporator. Residual solvent was removed under vacuum at room temperature.

**Table 1. PIB-Br Precursors**

| sample | $M_{n,GPC}$[a] (g/mol) | $M_{n,GPC}$[b] (g/mol) | $M_{n,NMR}$ (g/mol) | $M_w/M_n$ |
|---|---|---|---|---|
| $PIB_{44}$-Br | 2600 | 2600 | 2748 | 1.03 |
| $PIB_{71}$-Br | 4200 | 4000 | 4178 | 1.02 |
| $PIB_{95}$-Br | 5600 | 5500 | 5758 | 1.06 |

[a] $M_{n,GPC}$ determined using 100% mass recovery d$n$/d$c$. [b] $M_{n,GPC}$ determined using known d$n$/d$c$.

Each of three 1-(3-azidopropyl)pyrrole-terminated PIBs was prepared by reaction of the corresponding 1-(3-bromopropyl)-pyrrole-terminated PIB with $NaN_3$ in a mixture of heptane/DMF. A representative procedure to produce $PIB_{44}$-$N_3$ was as follows. To a 200 mL round-bottom flask, under a dry nitrogen atmosphere, were added 1-(3-azidopropyl)pyrrole-terminated $PIB_{44}$ (11.56 g, 4.4 mmol) and 25.5 mL of dry heptanes. The reaction vessel was agitated until complete dissolution of the $PIB_{44}$-$N_3$ occurred, resulting in a clear solution. To the resulting solution was then added a separate solution of sodium azide (0.853 g, 13.1 mmol) in 25.5 mL of DMF. After stirring for ~20 min, the resulting biphasic mixture was submerged in an oil bath at 90 °C and soon became monophasic as the reaction reached equilibrium temperature. The reaction was allowed to proceed with agitation for 17 h. Afterward, the monophasic reaction mixture was removed from the oil bath and allowed to cool to room temperature whereupon a biphasic mixture again formed. At this point, hexane and DI water were added, and the DMF/water layer was separated. The organic phase was immediately washed with DI water and then precipitated into methanol from hexane. The precipitate was collected by dissolution in hexane; the solution was washed with water, dried over $MgSO_4$, filtered, and concentrated on a rotatary evaporator. Residual solvent was removed under vacuum at room temperature.

**Synthesis of PIB-CTA by Click Chemistry.** To a 25 mL one-neck round-bottom flask equipped with a magnetic stir bar were added $PIB_{44}$-$N_3$ (2.032 g, 0.79 mmol) and 2.5 mL of THF. The reaction vessel was agitated until complete dissolution of the PIB-$N_3$ occurred, resulting in a clear solution. In a separate vessel, CTA (0.622 g, 1.55 mmol) and $(Ph_3P)_3CuBr$ (0.0515 g, 0.0554 mmol) were dissolved in 2.5 mL of THF, and the resulting solution was charged to the one-neck round-bottom flask. After 38 h, the solvent was removed under reduced pressure, and the crude product was redissolved in hexane. The resulting solution was washed with methanol three times, filtered, and precipitated twice into methanol from hexane. The precipitate was collected by dissolution in hexane and then stripped of solvent under reduced pressure until a constant weight was reached. A clear, yellow, viscous material was obtained.

**RAFT Polymerization of NIPAM with PIB-CTA.** A representative RAFT polymerization was conducted as follows. To a 25 mL Schlenk-style, long-neck round-bottom flask were added three

**Scheme 1. Synthesis of PIB-CTA for RAFT Polymerization**

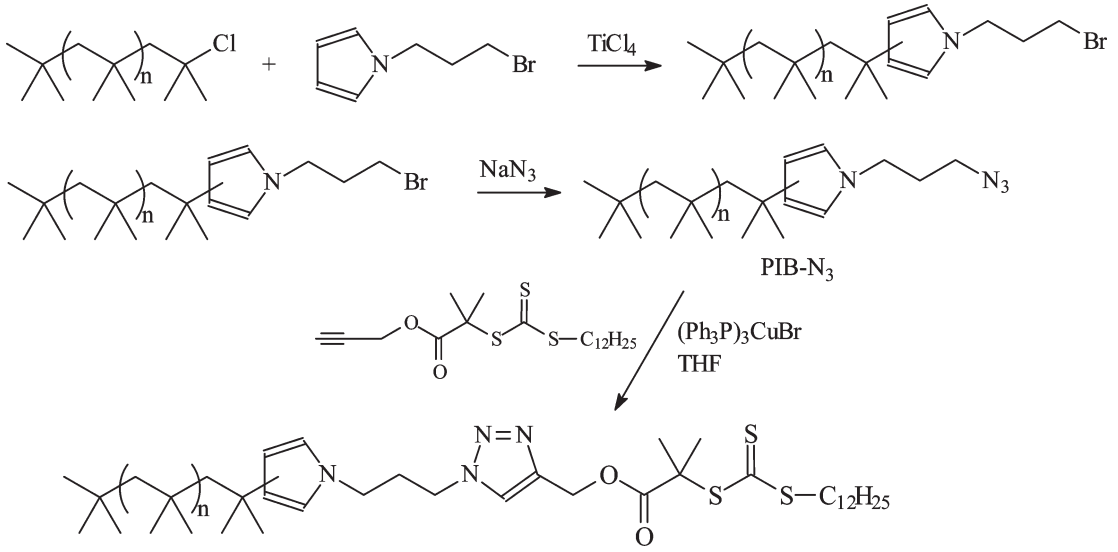


solutions: first a solution of $PIB_{44}$-CTA (0.0493 g, 0.0165 mmol) in 0.69 mL of heptane, a second solution of 1,3,5-trioxane (0.0458 g, 0.509 mmol) and NIPAM (0.5767 g, 5.0961 mmol) in 2.82 mL of dioxane, and a finally 0.5 mL of a 0.0099 M AIBN stock solution in dioxane. After mixing the three solutions an initial aliquot was taken to establish the initial monomer concentration relative to the internal standard 1,3,5-trioxane via $^1$H NMR spectroscopy. The solution was then subjected to three freeze−pump−thaw cycles to remove oxygen, sealed under $N_2$, and submerged in an oil bath thermostated at 85 °C. After ~4 h the reaction was exposed to oxygen and quenched in liquid nitrogen. A final aliquot was taken for $^1$H NMR analysis, and then the crude reaction product was precipitated into hexane twice, dialyzed against water, and lyophilized. Conversion was calculated from the initial and final monomer concentrations relative to 1,3,5-trioxane.

**Instrumentation.** NMR spectra were acquired using a Varian Mercury$^{plus}$ 300 MHz NMR spectrometer. Samples were dissolved in chloroform-*d* (3−7%, w/v) and analyzed using 5 mm NMR tubes.

Variable-temperature NMR (VT NMR) data were acquired using a $^{UNITY}$Inova 500 MHz NMR spectrometer equipped with a Highland VT controller. RAFT polymerizations were performed in dioxane-*d* between 355.5 and 363 K, with a 45 s preacquisition delay between each spectrum. The probe was allowed to equilibrate for 15 min prior to data acquisition. Temperatures reported in this study are within ±2 °C based on ethylene glycol calibration.[52,53] RAFT polymerizations for VT NMR were prepared by charging a J Young NMR tube equipped with a Teflon seal with the crude reaction mixture and performing three freeze−pump−thaw cycles. After degassing, the NMR tube was backfilled with $N_2$. Conversion was calculated by comparison of the vinyl proton areas of the monomer to the internal standard, 1,3,5-trioxane.

The number-average molecular weight ($M_n$) and polydispersity index (PDI) of the polymeric materials were measured using gel permeation chromatography (GPC). The GPC system, operating at 35 °C for PIB-Br, PIB-$N_3$, and PIB-CTA and 25 °C for PIB-*b*-PNIPAM, consisted of a Waters Alliance 2695 separations module, an online multiangle laser light scattering (MALLS) detector (MiniDAWN, Wyatt Technology Inc.), an interferometric refractometer (Optilab rEX, Wyatt Technology Inc.), an online differential viscometer (ViscoStar, Wyatt Technology, Inc.), and either two mixed E (3 μm bead size) or two mixed D (5 μm bead size) PL gel (Polymer Laboratories Inc.) GPC columns connected in series. Freshly distilled THF for PIB-homopolymer (PIB-Br, PIB-$N_3$, and PIB-CTA) and 0.25 wt % tetrabutylammonium bromide in THF (25 °C)[54] for PIB-*b*-PNIPAM served as the mobile phase at a flow rate of 1.0 mL/min. Sample concentrations were 10−12 mg/mL, with an injection volume of 100 μL. The detector signals were recorded using ASTRA software (Wyatt Technology Inc.) and molecular weights were determined using d*n*/d*c* values calculated from a known d*n*/d*c* equation reported elsewhere[51] or by the response of the Optilab DSP assuming 100% mass recovery from the columns.

Dynamic light scattering (DLS) was used to determine the hydrodynamic size of particles in aqueous solution as well as their distribution of sizes. Solutions of PIB-*b*-PNIPAM block copolymers were prepared by dissolving the polymer into purified water (Millipore) to a concentration of 0.01 wt %. Samples were agitated overnight to ensure complete dissolution and then filtered through a 0.22 μm PVDF syringe-driven filter (Millipore) directly into the scattering cell. Samples were then sonicated and allowed to equilibrate to temperature for 20 min prior to analysis. Scattering was performed using incident light at 633 nm from a Spectra Physics HeNe laser operating at 40 mW. For DLS, the angular dependence of the autocorrelation functions was measured using a Brookhaven BI-200SM goniometer with a TurboCorr correlator. Correlation functions were analyzed according to the method of cumulants using the companion software, from which a hydrodynamic diameter was extracted via the Stokes−Einstein relation. All data reported correspond to the average decay rate and normalized variance (polydispersity) obtained from the second-order cumulant fit.

## Results and Discussion

**Synthesis of PIB-CTA.** Site transformation of PIB into a macro-CTA for RAFT polymerization was accomplished using a click chemistry site transformation approach. This synthetic strategy, shown in Scheme 1, offers a number of advantages over our previously published method,[33] which involved quenching of quasiliving PIB with a hindered base to form *exo*-olefin PIB,[55] followed by hydroboration/oxidation to form hydroxyl-terminated PIB, followed finally by esterification with a carboxylic acid-functional trithiocarbonate CTA.[33] Most notably, in-situ quenching of quasiliving PIB with an N-substituted pyrrole provides higher chain-end functionality compared to the *exo*-olefin route, and the expensive and difficult hydroboration/oxidation reaction is eliminated.

As shown in Scheme 1, PIB-$N_3$ was synthesized in two steps. The first involved in-situ quenching of a $TiCl_4$-activated quasiliving cationic polymerization of IB with 1-(3-bromopropyl)-pyrrole to obtain the primary bromide-terminated PIB.[51] This

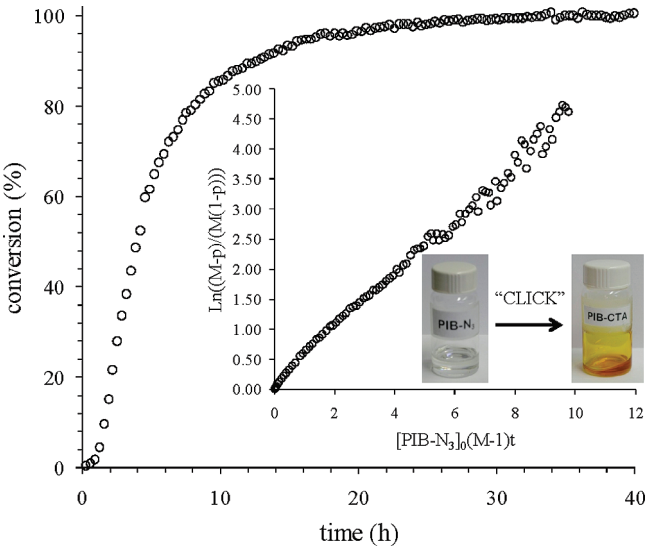


**Figure 1.** Real-time $^1$H NMR analysis of click reaction between CTA and PIB$_{44}$-N$_3$.

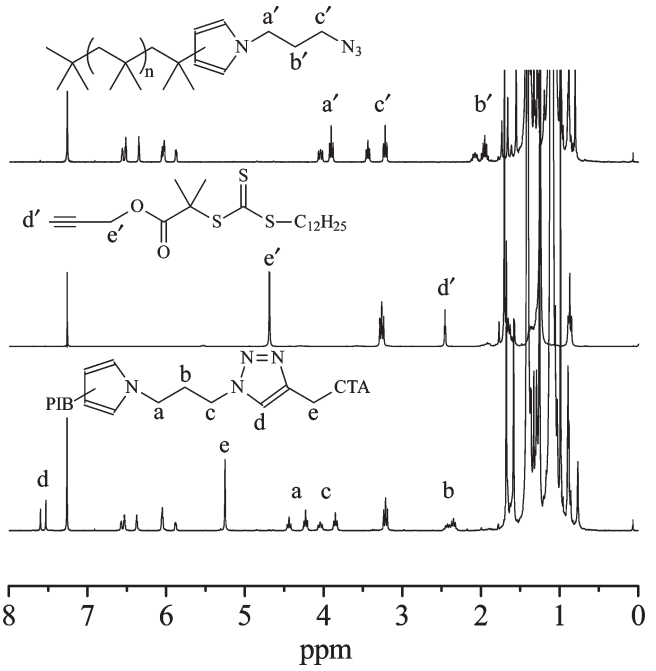


**Figure 2.** $^1$H NMR spectra of PIB-N$_3$ (top), CTA (middle), and PIB-CTA (bottom).

reaction was quantitative and yielded a mixture of two isomers, corresponding to attachment of the PIB chain at either the C2 or C3 position of the pyrrole ring. The C3 isomer was the major isomer and constituted about 60% of the chain ends. Table 1 lists molecular weights ($M_n$) and PDIs ($M_w/M_n$) of three bromide-functional PIBs synthesized by this method. This series of functional polymers was designed to probe the influence of PIB-CTA molecular weight on the RAFT polymerization of NIPAM and the properties of the resulting block copolymers. The results obtained from GPC and $^1$H NMR agree very well, differing by about 6% in the worst case. In addition, the PDIs were uniformly low. The second step involved displacement of the terminal bromide by azide ion via nucleophilic substitution. The reaction was biphasic at room temperature, with the hydrophobic PIB located in the top heptane layer and the polar sodium azide located in the bottom DMF layer. Upon heating, the reaction became homogeneous, and after ~12 h at 90 °C, complete substitution of the halogen to the terminal azide was accomplished without any noticeable coupling or loss of terminal functionality. Upon cooling, the layers separated once again, and this greatly facilitated removal of excess sodium azide and the byproduct sodium bromide.

The final step to create the PIB-CTA was the copper-catalyzed Huisgen cycloaddition reaction between PIB-N$_3$ and the alkyne-functionalized CTA (Scheme 1). The latter was synthesized by DCC/DMAP coupling as previously reported in the literature.[37] The azide−alkyne click reaction is attractive for the final coupling step since it can be carried out quantitatively at room temperature and in the presence of both oxygen and water. Conversion of PIB-N$_3$ into PIB-CTA (Figure 1) was monitored using real-time $^1$H NMR analysis by observing the decrease in area of the propargyl methylene proton signal of the CTA. Nearly 80% of the product was obtained after 8 h, whereas the remaining 20% required an additional 27 h to reach full conversion. Since both the CTA and PIB-N$_3$ had to be synthesized, it was impractical to use the former in large excess and thereby reduce the overall order of the reaction. Thus, the initial molar ratio ($M$) of alkyne to azide ([CTA]:[PIB-N$_3$]) was set only to 2. As expected under these conditions, the click reaction displayed second-order kinetics, as shown in the inset to Figure 1. Initial scouting experiments did reveal that the reaction rate can be dramatically increased by small increases in temperature (30−35 °C), higher catalyst concentrations, or by using a more reactive copper catalyst. Although full conversion takes ~35 h under these conditions, the simplicity and forgiving nature of the reaction make it very appealing. The product was purified by vacuum-stripping of THF, dissolution in hexane, and washing the resulting solution with methanol. The solution was then filtered to remove the copper catalyst, which has limited solubility in hexane, and finally, the polymer was isolated by precipitation into methanol, which also served to remove any residual catalyst and unreacted alkyne CTA. After removal of methanol, the purified PIB-CTA was a transparent yellow color instead of its originally colorless appearance, as shown in Figure 1.

The structure of PIB-CTA was confirmed by $^1$H NMR, FTIR, and GPC. Figure 2 shows $^1$H NMR spectra of the PIB-N$_3$ precursor (top), the alkyne CTA (middle), and the final PIB-CTA (bottom). A clear downfield shift of the PIB-N$_3$ tether protons (a′, b′, c′) and disappearance of the alkyne (d′) and methylene (e′) protons of CTA were observed upon triazole formation. No residual resonances from either PIB-N$_3$ or alkyne CTA were detectable in the resulting product, indicating quantitative functionalization. Formation of the triazole ring brings the alkyne proton into the general aromatic/heteroaromatic proton region. This proton (d) was observed as two separate peaks reflecting the mixture of 2-PIB and 3-PIB pyrrole isomers.

FTIR spectroscopy (Figure 3) clearly showed the disappearance of the azide at 2100 cm$^{-1}$ and the presence of three CTA frequencies representing the carbonyl, ester, and thiocarbonyl at approximately 1735, 1150 and 1124, and 1067 cm$^{-1}$, respectively. Further characterization with GPC (Figure 4) confirmed a small increase in molecular weight after coupling due to addition of the 403 g/mol CTA and absence of any chain extension or other side reactions as evidenced by a unimodal trace. Additionally, no detectable residual lower molecular weight PIB-N$_3$ was visible in the PIB-CTA trace.

**RAFT Polymerization of NIPAM.** After successful synthesis of PIB-CTA, it was employed in the RAFT polymerization of NIPAM, as depicted in Scheme 2. A mixed solvent system of dioxane/heptane was used to achieve a homogeneous reaction

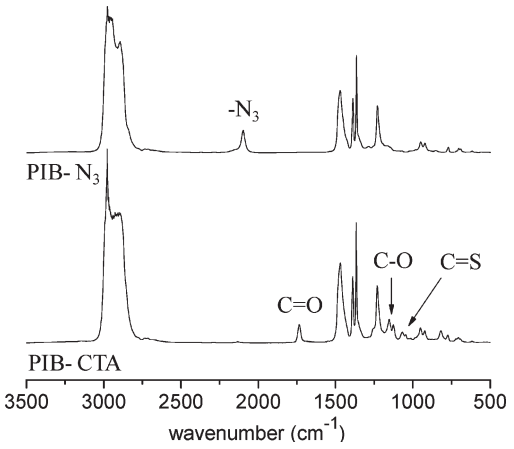


**Figure 3.** FTIR spectra of PIB-$N_3$ (top) and PIB-CTA (bottom).

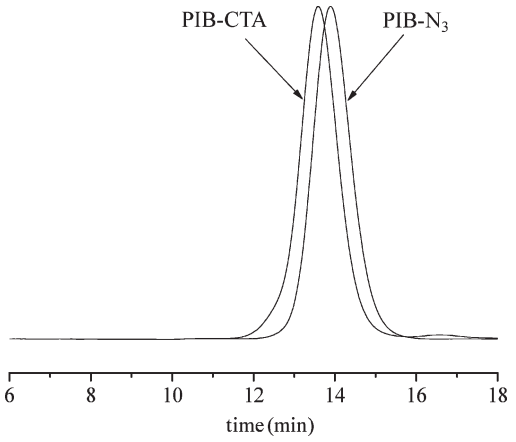


**Figure 4.** GPC trace before and after click reaction.

**Scheme 2. RAFT Polymerization of NIPAM with PIB-CTA**

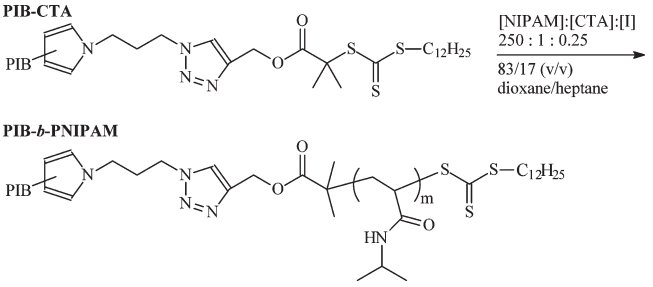


medium. For some formulations, the reaction was slightly heterogeneous upon initial mixing at room temperature, but the system became homogeneous after submerging the reaction in an oil bath during polymerization. It should also be noted that dissolution of the PIB-CTA in heptane prior to its addition to the other reagents added in its facile solvation substantially.

Table 2 summarizes the results of RAFT polymerizations formulated using various combinations of PIB-CTA molecular weight ($\overline{M}_{n,PIB\text{-}CTA}$), [NIPAM]:[CTA] ratio, and NIPAM fractional conversion ($p_{NIPAM}$), conducted to demonstrate control of both the PIB and PNIPAM block lengths. The theoretical degree of polymerization of the PNIPAM block ($\overline{X}_{n,theo}$) was targeted as $p_{NIPAM}$[NIPAM]/[CTA]. Reactions R1−R3 employed the same PIB-CTA and targeted different $\overline{X}_{n,theo}$ ranging from approximately 190 to 370. Experiments R3 through R5 utilized three different PIB-CTA molecular weights ranging from approximately 3000 to 6000 g/mol. In all cases, good to excellent agreement was observed between theoretical and experimental degree of polymerization of the PNIPAM block ($\overline{X}_{n,GPC}$), and the resulting diblock copolymers all possessed narrow PDI.

The resulting block copolymers were characterized using $^1$H NMR and GPC. $^1$H NMR (Figure 5) shows clear, strong resonances from both segments of the block copolymer. PIB backbone resonances are identified "a" and "b" while the PNIPAM resonances are labeled "c" through "g". Purification of the block copolymer was accomplished by precipitation into hexane, for removal of residual PIB-CTA, and dialysis against water for removal of unreacted NIPAM. A representative GPC trace, Figure 6, shows lower elution time of the block copolymer in comparison to the PIB-CTA homopolymer, indicative of increased molecular weight of the former. Moreover, the crude GPC trace shows a small amount of residual PIB-CTA and its effective removal by the hexanes precipitation.

**RAFT Polymerization Kinetics.** Kinetics of RAFT polymerizations from various PIB-CTA was monitored using variable temperature real-time $^1$H NMR. Figure 7 shows the temperature dependence of the RAFT polymerization with a NIPAM concentration of 1.2 M and [NIPAM]:[CTA]:[I] = 250:1:0.25. After a characteristic induction period, the polymerizations were first-order up to $p_{NIPAM} \approx 0.7$, indicating a constant concentration of actively propagating radicals, whereas at higher conversions the plots displayed a slight downward curvature, implying a decreasing concentration of active species. Eventually, a maximum conversion was reached beyond which no further polymerization occurred; for the higher polymerization temperatures this was at $p_{NIPAM} \approx 0.9$. The apparent first-order rate constants, $k_{app}$, extracted from the linear portion of the plots, were fitted to the Arrhenius equation (Figure A, Supporting Information) to yield an activation energy of 31.0 kcal/mol and a prefactor of $2.71 \times 10^{17}$ min$^{-1}$. This is very close to the reported activation energy for AIBN dissociation and confirms the strong effect of reaction temperature on polymerization rate. In addition, the duration of the induction period decreased with increasing temperature and was practically eliminated at 90 °C.

The kinetics and energetics information obtained in the VT NMR experiments were consistent with RAFT polymerization kinetics observed in the batch reactions of Table 2. For the latter, the external bath temperature was 85 °C; however, the internal reactor temperature was typically only 78−79 °C, after a thermal equilibration period of about 15−20 min. A replicate of experiment R2 was performed in which aliquots were removed for conversion analysis using $^1$H NMR. The data revealed first-order kinetics ($k_{app} = 0.0127$ s$^{-1}$) and an induction period of 50 min (taken as the $x$-intercept from the first-order plot). This $k_{app}$ value agrees very well with that predicted from the Arrhenius relationship ($k_{app} = 0.0139$ s$^{-1}$) above for a reaction temperature of 78 °C. The previously mentioned Arrhenius relationship and experimentation help to verify the slower reaction rate observed for the batch reaction, specifically R2, which accounts for it achieving a lower than expected conversion value ($p_{NIPAM} = 0.376$). Using either of the above rate constants and the empirically determined induction period, theoretical conversion values between 0.32 and 0.34 can be calculated which fall in close proximity to the experimental conversion value of R2.

Figure 8 shows the dependence of RAFT polymerization kinetics on the concentration of the thermal initiator AIBN. The maximum conversion achieved in the polymerization decreased with lower concentrations of initiator, from just

**Table 2. RAFT Polymerization Data[a]**

| | RAFT polymerization conditions | | | | PNIPAM block | | PIB-*b*-PNIPAM | | |
|---|---|---|---|---|---|---|---|---|---|
| sample | $\overline{M}_{n,PIB\text{-}CTA}$[b] (g/mol) | [NIPAM]:[CTA]:[I] | time (h) | $p_{NIPAM}$ | $\overline{X}_{n,Theo}$[c] | $\overline{X}_{n,GPC}$[d] | $\overline{M}_{n,Theo}$[e] (g/mol) | $\overline{M}_{n,GPC}$[f] (g/mol) | PDI |
| R1 $PIB_{44}$-*b*-$PNIPAM_{500}$ | 2990 | 487:1:0.5 | 4.00 | 0.766 | 373 | 328 | 45 199 | 40 100 | 1.08 |
| R2 $PIB_{44}$-*b*-$PNIPAM_{188}$ | 2990 | 492:1:0.5 | 1.33 | 0.376 | 185 | 193 | 23 925 | 24 800 | 1.04 |
| R3 $PIB_{44}$-*b*-$PNIPAM_{300}$ | 2990 | 309:1:0.3 | 4.00 | 0.760 | 235 | 210 | 29 583 | 26 700 | 1.02 |
| R4 $PIB_{71}$-*b*-$PNIPAM_{300}$ | 4535 | 292:1:0.3 | 4.00 | 0.795 | 232 | 197 | 30 788 | 26 800 | 1.03 |
| R5 $PIB_{95}$-*b*-$PNIPAM_{300}$ | 5959 | 288:1:0.3 | 4.00 | 0.813 | 234 | 236 | 32 438 | 32 700 | 1.05 |
| R6 $PIB_{44}$-*b*-$PNIPAM_{450}$ | 2990 | 485:1:0.5 | 8.00 | 0.887 | 431 | 450 | 51 762 | 53 200 | 1.09 |

[a] Stirred glass reactors; temperature (external bath) = 85 °C, internal reactor temperature = 78−79 °C; [NIPAM] = 1.2 M. [b] $\overline{M}_{n,PIB\text{-}CTA} = \overline{M}_{n,PIB\text{-}Br}$ (100% mass recovery d$n$/d$c$) + ($MW_{N3} - MW_{Br}$) + $MW_{CTA}$. [c] $\overline{X}_{n,theo} = p_{NIPAM}$[NIPAM]/[CTA]. [d] $\overline{X}_{n,GPC} = (\overline{M}_{n,GPC} - \overline{M}_{n,PIB\text{-}CTA})/MW_{NIPAM}$. [e] $\overline{M}_{n,Theo} = \overline{M}_{n,PIB\text{-}CTA} + \overline{X}_{n,Theo} \times MW_{NIPAM}$. [f] $\overline{M}_{n,GPC}$ determined using 100% mass recovery d$n$/d$c$.

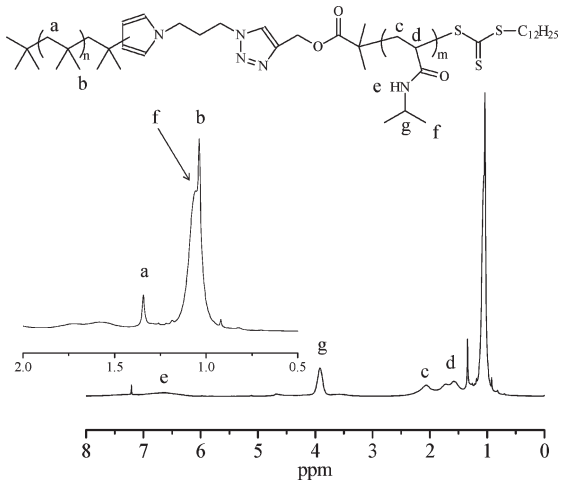


**Figure 5.** $^1$H NMR spectrum of PIB-*b*-PNIPAM (R2, Table 2).

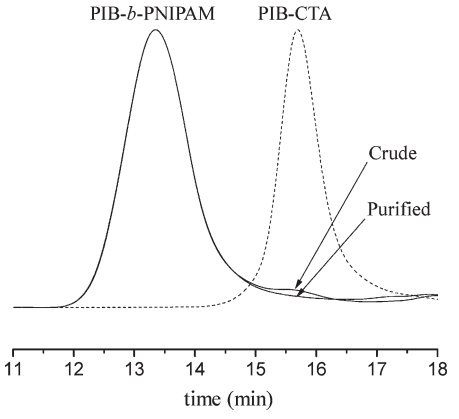


**Figure 6.** GPC traces before and after RAFT polymerization of PNIPAM (R2, Table 2).

over 0.9 at [CTA]:[I] = 0.25 to ~0.73 at [CTA]:[I] = 0.125. In addition, increasing initiator concentration reduced the duration of the induction period and increased the apparent rate constant of the polymerization, as expected.

Conversion and rate of RAFT polymerizations were observed to be independent of both PIB-CTA molecular weight and concentration (see Figures B and C, Supporting Information).

**Aqueous Self-Assembly of PIB-*b*-PNIPAM.** Below the critical point of PNIPAM (ca. 32 °C), amphiphilic PIB−PNIPAM block copolymers are expected to self-assemble into higher-ordered structures. In addition, these structures are expected to show temperature-dependent dimensions near the critical point for PNIPAM. The self-assembly and

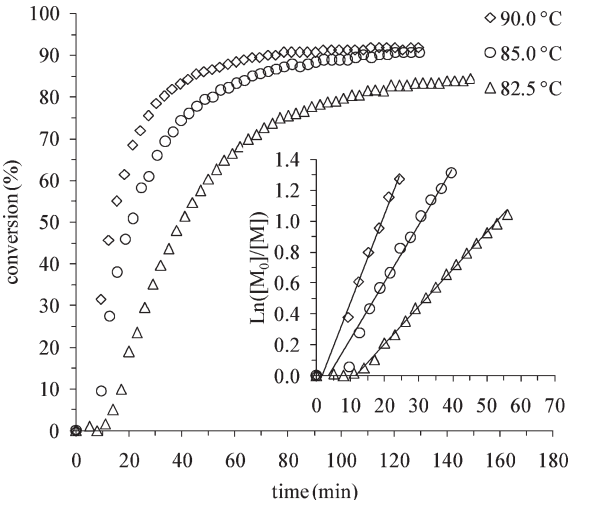


**Figure 7.** Conversion vs time and first-order kinetic plot (inset) for RAFT polymerization from $PIB_{44}$-CTA as a function of temperature. [NIPAM] = 1.2 M; [NIPAM]:[CTA]:[I] = 250:1:0.25.

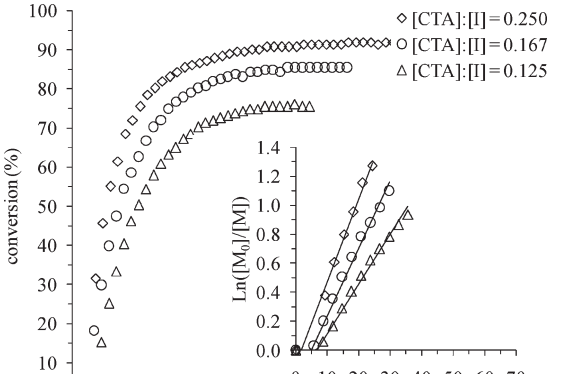


**Figure 8.** Conversion vs time and first-order kinetic plot (inset) for RAFT polymerization from $PIB_{44}$-CTA as a function of thermal initiator concentration. [NIPAM] = 1.2 M; [NIPAM]:[CTA] = 250:1; $T$ = 90 °C.

temperature responsiveness for $PIB_{44}$-$PNIPAM_{450}$ (R6 from Table 1) was studied using DLS. On the basis of the large weight fraction of hydrophilic PNIPAM, it is expected that spherical micelles will form.[56] At room temperature, direct solvation of $PIB_{44}$-$PNIPAM_{450}$ resulted in a clear solution (Figure 9). The correlation functions fit well to a second-order cumulant relation, indicative of a relatively monodisperse, unimodal distribution of scattering species.

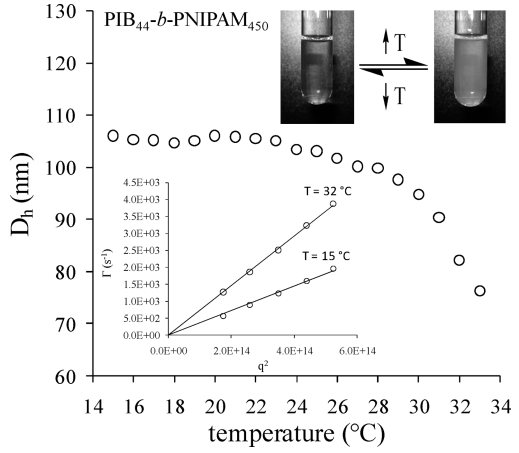


**Figure 9.** Hydrodynamic diameter of micelles with temperature ($\theta = 90°$).

A plot of the average decay rate of the correlation function ($\Gamma$) vs the square of the scattering vector ($q^2$) yielded a linear relation (Figure 9 inset), indicating that the scattering comes solely from Brownian motion of spherical aggregates.

The hydrodynamic diameter ($D_h$) was determined as a function of temperature at a 90° scattering angle. At 15 °C, the $D_h$ was 107 nm. As the temperature increased, the hydrodynamic size remained relatively constant until 26 °C where it began to decrease. When the temperature was further increased toward the nominal critical point of PNIPAM, the aggregate diameter continued decreasing to 76 nm. The decrease in size with increased temperature is explained by the PNIPAM chains transforming from a coil to a globular conformation.[57] This conformational change results in the expulsion of water due to the increased hydrophobicity of the PNIPAM corona chains. It is important to note that the overall structure of the aggregates does not change over the temperature range studied, i.e., the $\Gamma$ vs $q^2$ plot retains linearity over the temperature range, suggesting that spherical aggregates are still present at 32 °C (Figure 9, inset). In addition, the polydispersity (normalized variance) in the size distribution systematically decreased from 0.187 to 0.133 as temperature increased from 15 to 33 °C. Finally, a fairly broad transition ranging from 26 to 33 °C occurs with $PIB_{44}$-*b*-$PNIPAM_{450}$ block copolymer, in contrast to sharp transitions which occur in PNIPAM homopolymer systems.[42] Broadened PNIPAM transitions are theoretically expected with hydrophobically modified PNIPAM[58] and have been observed with PS-*b*-PNIPAM systems.[59] Once the temperature of the system exceeded 33 °C, intermolecular aggregation occurred between assemblies, which was accompanied by a visual change in the aqueous solution from transparent to turbid (Figure 9).

## Conclusion

A novel block copolymer composed of PIB and PNIPAM block segments was synthesized by a unique site transformation process combining quasiliving cationic and RAFT polymerizations. PIB with a terminal halogen was functionalized by in-situ quenching and successfully converted into a "clickable" PIB by substitution with azide ion. Afterward, the azido-functionalized PIB was transformed into a macro-CTA by copper-catalyzed click chemistry utilizing an alkyne-functionalized CTA. The utility of the macro-CTA was demonstrated by polymerization of NIPAM to produce a novel block copolymer with predetermined molecular weights and low PDIs. The kinetic behavior of this RAFT polymerization was studied and found to be strongly dependent on temperature and initiator concentration. Conversely, the PIB-CTA molecular weight and concentration had little effect on the kinetic behavior. Light scattering experiments confirmed the presence of polymeric aggregates with stimuli-responsive behavior, displaying a broad temperature-induced transition.

**Supporting Information Available:** Plot of $\ln k_{app}$ for RAFT polymerization vs reciprocal temperature (Figure A); conversion vs time and first-order kinetic plot for RAFT polymerization as a function of PIB-CTA molecular weight (Figure B) and PIB-CTA concentration (Figure C). This material is available free of charge via the Internet at http://pubs.acs.org.

## References and Notes

(1) Matyjaszewski, K. *Prog. Polym. Sci.* **2005**, *30*, 858–875.
(2) Ruzette, A.; Leibler, L. *Nat. Mater.* **2005**, *4*, 19–31.
(3) Lindman, B.; Alexandridis, P. In *Amphiphilic Block Copolymers: Self Assembly and Applications*, 1st ed.; Elsevier Science B. V.: Dordrecht, The Netherlands, 2000; Chapter 15, pp 347−376.
(4) Kopecek, J. *Nature* **2002**, *417*, 388–391.
(5) Jeong, B.; Bae, Y. H.; Lee, D. S.; Kim, S. W. *Nature* **1997**, *388*, 860–862.
(6) McIlroy, D.; Barteau, B.; Cany, J.; Richard, P.; Gourden, C.; Conchon, S.; Pitard, B. *Mol. Ther.* **2009**, doi: 10.1038/mt.2009.84.
(7) Pinchuk, L.; Wilson, G. J.; Barry, J. J.; Schoephoerster, R. T.; Parel, J. M.; Kennedy, J. P. *Biomaterials* **2008**, *29*, 448–460.
(8) Place, E. S.; Evans, N. D.; Stevens, M. M. *Nat. Mater.* **2009**, *8*, 457–470.
(9) Hadjichristidis, N.; Pispas, S.; Floudas, G. A. In *Block Copolymers: Synthetic Strategies, Physical Properities, and Applications*, 1st ed.; John Wiley & Sons: New York, 2002; Chapter 21, pp 383−406.
(10) Diat, O.; Gebel, G. *Nat. Mater.* **2008**, *7*, 13–14.
(11) Lazzari, M.; Liu, G.; Lecommandoux, S. In *Block Copolymers in Nanoscience*, 1st ed.; Wiley-VCH: Weinheim, 2006; Chapter 15, pp 337−366.
(12) Tang, C.; Lennon, E. M.; Fredrickson, G. H.; Kramer, E. J.; Hawker, C. J. *Science* **2008**, *322*, 429–432.
(13) Ryan, A. *Nature* **2008**, *456*, 334–336.
(14) Ranade, S. V.; Miller, K. M.; Richard, R. E.; Chan, A. K.; Allen, M. J.; Helmus, M. N. *J. Biomed. Mater. Res.* **2004**, *71A*, 625–634.
(15) Pinchuk, L. U.S. Patent 5,741,331, 1998.
(16) Fray, M. E.; Prowans, P.; Puskas, J. E.; Altstadt, V. *Biomacromolecules* **2006**, *7*, 844–850.
(17) Binder, W. H.; Sachsenhofer, R. *Macromol. Rapid Commun.* **2008**, *29*, 1097–1103.
(18) Nagy, M.; Szollosi, L.; Keki, S.; Faust, R.; Zsuga, M. *J. Macromol. Sci., Part A: Pure Appl. Chem.* **2009**, *46*, 331–338.
(19) Burkhardt, M.; Ruppel, M.; Tea, S.; Drechsler, M.; Schweins, R.; Pergushov, D. V.; Gradzielski, M.; Zezin, A. B.; Mueller, A. H. E. *Langmuir* **2008**, *24*, 1769–1777.
(20) Jewrajka, S. K.; Yilgor, E.; Yilgor, I.; Kennedy, J. P. *J. Polym. Sci., Part A: Polym. Chem.* **2008**, *47*, 38–48.
(21) Jewrajka, S. K.; Kang, J.; Erdodi, G.; Kennedy, J. P. *J. Polym. Sci., Part A: Polym. Chem.* **2009**, *47*, 2787–2797.
(22) Binder, W. H.; Machl, D. *J. Polym. Sci., Part A: Polym. Chem.* **2005**, *43*, 188–202.
(23) Puskas, J. E.; Dos Santos, L. M.; Kaszas, G.; Kulbara, K. *J. Polym. Sci., Part A: Polym. Chem.* **2009**, *47*, 1148–1158.
(24) Zhu, Y.; Storey, R. F. *Polym. Prepr.* (*Am. Chem. Soc., Div. Polym. Chem.*) **2009**, *50* (2), 535–536.
(25) Kwon, Y.; Faust, R. *Adv. Polym. Sci.* **2004**, *167*, 107–135.
(26) Takacs, A.; Faust, R. *Macromolecules* **1995**, *28*, 7266–7270.
(27) Jakubowski, W.; Tsarevsky, N. V.; Higashihara, T.; Faust, R.; Matyjaszewski, K. *Macromolecules* **2008**, *41*, 2318–2323.
(28) Storey, R. F.; Scheuer, A. D.; Achord, B. C. *Polymer* **2005**, *46*, 2141–2152.
(29) Breland, L. K.; Murphy, J. C.; Storey, R. F. *Polymer* **2006**, *47*, 1852–1860.
(30) Zaschke, B.; Kennedy, J. P. *Macromolecules* **1995**, *28*, 4426–4432.
(31) Martinez-Castro, N.; Lanzendorfer, M. G.; Muller, A. H. E.; Cho, J. C.; Acar, M. H.; Faust, R. *Macromolecules* **2003**, *36*, 6985–6994.
(32) Feng, D.; Higashihara, T.; Faust, R. *Polymer* **2008**, *49*, 386–393.
(33) Magenau, A. J. D.; Martinez-Castro, N.; Storey, R. F. *Macromolecules* **2009**, *42*, 2353–2359.
(34) Moad, G.; Chong, Y. K.; Postma, A.; Rizzardo, E.; Thang, S. H. *Polymer* **2005**, *46*, 8458–8468.

(35) Moad, G.; Rizzardo, E.; Thang, S. H. *Polymer* **2008**, *49*, 1079–1131.
(36) Gondi, S. R.; Vogt, A. P.; Sumerlin, B. S. *Macromolecules* **2007**, *40*, 474–481.
(37) Ranjan, R.; Brittain, W. J. *Macromolecules* **2007**, *40*, 6217–6223.
(38) Kolb, H. C.; Finn, M. G.; Sharpless, K. B. *Angew. Chem., Int. Ed.* **2001**, *40*, 2004–2021.
(39) Rostovtsev, V. V.; Green, L. G.; Fokin, V. V.; Sharpless, K. B. *Angew. Chem., Int. Ed.* **2002**, *114*, 2708–2711.
(40) Lodge, L. P. *Macromolecules* **2009**, *42*, 3827–3829.
(41) Ballauff, M.; Lu, Y. *Polymer* **2007**, *48*, 1815–1823.
(42) Schild, H. G. *Prog. Polym. Sci.* **1992**, *17*, 163–249.
(43) Yamazaki, A.; Song, J. M.; Winnik, F. M.; Brash, J. L. *Macromolecules* **1998**, *31*, 109–115.
(44) Wei, H.; Zhang, X.; Cheng, C.; Cheng, S.; Zhou, R. *Biomaterials* **2007**, *28*, 99–107.
(45) Zhou, X.; Ye, X.; Zhang, G. *J. Phys. Chem. B* **2007**, *111*, 5111–5115.
(46) Nuopponen, M.; Ojala, J.; Tenhu, H. *Polymer* **2004**, *45*, 3643–3650.
(47) Klaikherd, A.; Nagamani, C.; Thayumanavan, S. *J. Am. Chem. Soc.* **2009**, *131*, 4830–4838.
(48) Schild, H. G.; Tirrell, D. A. *Langmuir* **1991**, *7*, 1319–1324.
(49) Kujawa, P.; Segui, F.; Shaban, S.; Diab, C.; Okada, Y.; Tanaka, F.; Winnik, F. M. *Macromolecules* **2006**, *39*, 341–348.
(50) Yamazaki, A.; Song, J.; Winnink, F.; Brash, J. L. *Macromolecules* **1998**, *31*, 109–115.
(51) Martinez-Castro, N.; Morgan, D. L.; Storey, R. F. *Macromolecules* **2009**, *42*, 4963–4971.
(52) English, A. D. *J. Magn. Reson.* **1984**, *57*, 491–493.
(53) Van Geet, A. L. *Anal. Chem.* **1968**, *40*, 2227–2229.
(54) Schilli, C.; Lanzendorfer, M. G.; Muller, A. H. E. *Macromolecules* **2002**, *35*, 6819–6827.
(55) Simison, K. L.; Stokes, C. D.; Harrison, J. J.; Storey, R. F. *Macromolecules* **2006**, *39*, 2481–2487.
(56) Discher, D. E.; Ahmed, F. *Annu. Rev. Biomed. Eng.* **2006**, *8*, 323–341.
(57) Wang, X.; Wu, C. *Macromolecules* **1999**, *32*, 4299–4301.
(58) Zhulina, E. B.; Borisov, O. V.; Pryamitsyn, V. A.; Birshtein, T. M. *Macromolecules* **1991**, *24*, 140–149.
(59) Zhang, W.; Zhou, X.; Li, H.; Fang, Y.; Zhang, G. *Macromolecules* **2005**, *38*, 909–914.